Polysulfone nanofiber-modified composite laminates

Investigation of mode-I fatigue behavior and damage mechanisms

Mohammadi, Reza; Akrami, Roya; Assaad, Maher; Nasor, Mohamed; Imran, Ahmed; Fotouhi, Mohammad

DOI
10.1016/j.tafmec.2023.104078

Publication date
2023

Document Version
Final published version

Published in
Theoretical and Applied Fracture Mechanics

Citation (APA)
Mohammadi, R., Akrami, R., Assaad, M., Nasor, M., Imran, A., & Fotouhi, M. (2023). Polysulfone nanofiber-modified composite laminates: Investigation of mode-I fatigue behavior and damage mechanisms. *Theoretical and Applied Fracture Mechanics*, *127*, Article 104078. https://doi.org/10.1016/j.tafmec.2023.104078

Theoretical and Applied Fracture Mechanics 127 (2023) 104078

Contents lists available at ScienceDirect

Theoretical and Applied Fracture Mechanics

journal homepage: www.elsevier.com/locate/tafmec

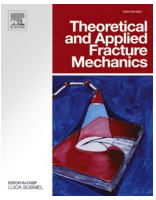

Polysulfone nanofiber-modified composite laminates: Investigation of mode-I fatigue behavior and damage mechanisms

Reza Mohammadi [a,*], Roya Akrami [b], Maher Assaad [c], Mohamed Nasor [d], Ahmed Imran [d], Mohammad Fotouhi [a]

[a] Faculty of Civil Engineering and Geosciences, Delft University of Technology, 2628 CD Delft, the Netherlands
[b] Department of Mechanical and Aerospace Engineering, University of Strathclyde, 75 Montrose Street, Glasgow G1 1XJ, UK
[c] Department of Electrical and Computer Engineering, College of Engineering and IT, Ajman University, Ajman P.O. Box 346, United Arab Emirates
[d] Department of Biomedical Engineering, College of Engineering and IT, Ajman University, Ajman P.O. Box 346, United Arab Emirates

ARTICLE INFO

Keywords:
Carbon/epoxy
Polysulfone nanofiber
Electro spinning process
Fatigue crack growth rate
Fracture toughness

ABSTRACT

In this study, the fatigue properties of carbon fiber-reinforced polymer (CFRP) composite laminates were investigated, specifically focusing on the incorporation of 100-μm polysulfone (PSU) nanofibers as an interleaving material. The PSU nanofibers were produced using the electrospinning technique. Both quasi-static and fatigue tests were conducted on both the reference specimens and the modified specimens to evaluate their mode-I performance. The results revealed an 85% increase in fracture toughness (G_{IC}) under quasi-static testing. The fatigue plots revealed a noteworthy reduction in the fatigue crack growth rate (da/dN) for the modified specimens due to new toughening mechanisms. Scanning electron microscopy (SEM) demonstrated that, the PSU nanofiber became melted and distributed in the interface, leading to phase separation and a sea-island structure. The presence of PSU microspheres caused crack deflection during delamination, which resulted in increased fracture and fatigue resistance.

1. Introduction

Over the past few decades, composite laminates have been widely used in various industrial sectors, including aerospace and wind energy systems, owing to their exceptional strength-to-weight ratio. Composite laminates are composed of at least two fundamental constituents: reinforcement, which includes materials like carbon fiber, glass fiber, etc., and matrix, such as thermoplastic and thermoset polymers. Thermoset resins, such as epoxy, are commonly utilized as matrices in these materials due to their numerous benefits, including excellent mechanical performance and low density. However, the brittle nature of thermosets can render laminated composites susceptible to delamination under mechanical loadings [1–4].

Delamination is a commonly observed failure mechanism that typically originates from in-plane cracks and subsequently propagates, leading to fracture and ultimate failure [5–8]. In the past few decades, nanofibers have emerged as a significant technological advancement that has found extensive applications across various research and industrial sectors. One notable applications of nanofibers is their use as toughening agents in composite laminates, offering remarkable efficacy in delamination prevention [9–12]. The unique morphology of nanofibrous mats makes them ideal for embedding between two plies of a laminate, prompting extensive research efforts to investigate their profound influence on the overall behavior of composite laminates [9,13]. Different types of polymers, such as polyvinylidene fluoride (PVDF) [14], Nitrile Butadiene Rubber [15] polyvinyl butyral (PVB) [1,16,17], polysulfone (PSU) [18,19], polycaprolactone (PCL) [20–22], and nylon [23–29] have been utilized as toughening nanofibers between composite layers.

Based on the toughening mechanisms, the polymeric nanofibers used for enhancing interlayer adhesion in composites can be broadly categorized into two types:

- Type 1, where nanofibers retain their original structure and morphology after the resin has fully cured. Throughout the laminating and subsequent curing process, the nanofibers undergo minimal alterations to their initial shape and structure. The resin effectively penetrates the pores of the nanofibers, ensuring thorough

* Corresponding author.
E-mail address: Rezam75@gmail.com (R. Mohammadi).

https://doi.org/10.1016/j.tafmec.2023.104078
Received 19 June 2023; Received in revised form 29 August 2023; Accepted 3 September 2023
Available online 6 September 2023

impregnation and integration with the nanofiber network. In this scenario, researchers [30,31] have identified the bridging effect of the nanofibers between the layers as the primary mechanism responsible for the enhanced toughness observed.

- Type 2, where nanofibers undergo structural changes during the composite fabrication process and curing at elevated temperatures. The increased temperature and the exothermic heat generated by the resin during the curing process cause the nanofibers to melt and disperse within the composite matrix.

It is worth emphasizing that the classification of a specific type of nanofiber can vary depending on the matrix resin employed and its corresponding curing temperature. For instance, in a research conducted by Saghafie et al. [25], PVDF nanofiber was utilized as Type 2 for toughening composite materials. This process entailed the use of an epoxy resin with a curing temperature exceeding the melting point of PVDF, resulting in the melting of PVDF nanofibers and subsequent changes in their morphology. On the other hand, in a separate study by Magniez et al. [32], PVDF was classified as Type 1, where the temperature of curing process was lower than the melting point of nanofiber, resulting in no significant change in the morphology of PVDF.

There have been some studies on evaluating the performance of the type 1 modified composites, both for static and fatigue behavior under different delamination loading conditions. For example, Brugo et al. [13] used PA 6,6 nanofibers to consider the fatigue properties of CFRP Laminates under Mode-I loading condition. Their findings revealed significant enhancements in delamination resistance for the modified specimens. The delamination toughness experienced a significant increase of 130%, and the propagation of cracks occurred at a significantly slower rate (36–27 times slower) compared to the reference one. However there has been little research on the effect of type 2 nanofibers, which undergo structural changes during the curing process, on delamination behavior of modified composites. Recent studies [33,34] have been dedicated to exploring the mode-I and mode-II static loading conditions in the context of this subject matter. Their observations revealed that when the curing temperature of composite laminates surpassed the melting point of the nanofibers (such as PVDF and PSU), the nanofibers underwent a melting phase. The porous structure of the nanofibrous mats enabled the epoxy to permeate completely, leading to a thorough blending with the nanofiber mats during the curing process. Due to the thermoplastic nature of nanofibers and their inherent higher toughness compared to thermosets matrix like epoxy, the presence of nanofiber/epoxy blends demanded a greater amount of energy for crack propagation.

To the author's best knowledge there has been no study on the mode-I fatigue behavior of the type 2 nanofibers and the morphology of the associated failure mechanisms. Therefore, in this research, the use of PSU nanofibers, a type 2 nanofiber as a toughening agent for carbon/epoxy composites, was investigated for the first time for its effectiveness in enhancing the fatigue properties. The quasi-static tests revealed an 85% enhancement in mode-I fracture toughness (G_{IC}) for the modified specimens. Moreover, the fatigue crack growth rate in the modified specimens exhibited a substantial reduction, reaching up to 22 times compared to the unmodified specimens. Lastly, scanning electron microscopy (SEM) was employed to analyze the fractured surface of the laminates, aiming to investigate the toughening mechanisms. The SEM analysis revealed that the inclusion of PSU nanofibers effectively mitigated fatigue failure mechanisms, including scarp lines, striation patterns, and fiber–matrix debonding. Consequently, the rate of fatigue crack growth was significantly reduced.

This manuscript comprises seven distinct sections, which are: 1-Introduction 2- Specimen Manufacturing 3-Testing procedures 4- Quasi-static results 5- Fatigue test results 6- SEM results and 7- Conclusion. Additionally, the paper concludes with sections dedicated to Acknowledgments and References.

2. Specimen manufacturing

2.1. Production of PSU nanofiber

In this study, the electrospinning technique was employed to produce nanofibers. Pellets of PSU polymer were utilized as the source material for the fabrication of the nanofibers. Udel® 3500, which has the following properties: density of 1.24 g/cm3, melting point of 316–371 °C, and tensile strength of 70.3 MPa (provided by Solvay company website). The solution was prepared by dissolving 25 g of polysulfone in a 100 ml solvent (see Fig. 1 to more detail). To achieve a uniform nanofibrous mat with a targeted thickness of 100 ± 5 μm, the solution underwent electrospinning using specific parameters. These parameters included an applied voltage of 27 kV, a feed rate of 1.4 ml/h, and a distance of 14 cm between the needle tip and collector.

2.2. Lamination of composite specimens

The fabrication steps and test method are presented in Fig. 2. The AS4/8552 prepreg material was used to create composite plates (Fig. 2-A). During the laminating process, a total of 24 layers were stacked, and a thin Teflon film was inserted between the mid-plies to introduce a pre-crack. Then the PSU nanofiber was positioned at the edge of the Teflon film, serving as a pre-crack initiator as shown in Fig. 2-B. The laminated specimens were subjected to a curing process in an autoclave, as illustrated in Fig. 2-C, following the guidelines provided in the prepreg datasheet [35]. Following the guidelines outlined in the provided data sheet, the curing process commences by situating the samples inside an autoclave. Subsequent to this step, the initial action entails elevating the autoclave's pressure to 7 bars. Subsequently, the temperature is progressively heightened until it reaches 110 ℃, which is then maintained for a duration of 60 min. In the subsequent phase, the temperature is further raised until it reaches 180 ℃, and this elevated temperature is sustained for a period of 120 min. Finally, a gradual reduction in the autoclave temperature ensues, gradually reaching room temperature. Once this is achieved, the pressure within the autoclave is released.

After the composite plates were prepared, specimens were cut to dimensions of 180 mm in length and 25 mm in width using a grinding machine. To prepare the samples for mode-I testing, two aluminum blocks were securely attached to both sides of each sample using epoxy glue (Fig. 2-D).

3. Testing procedures

This section outlines the methodology for fracture and fatigue testing, which follows standard test methods. The following subsections provide detailed information on the testing procedures for fracture and fatigue.

3.1. Quasi-static test

The fracture testing was conducted following the guidelines outlined in the ASTM D5528 [36] standard. The specimens were subjected to displacement-controlled loading at a constant rate of 1 mm/min. Throughout the test, the displacement and load values were continuously monitored, and the growth of crack was recorded using a digital camera, as depicted in Fig. 3. Prior to conducting the tests, calibration of the testing machine was performed. The load cell and displacement measurements of the machine exhibited a relative error of 0.8% and 1%, respectively. To ensure repeatability, three specimens of each specimen type (Reference and PSU-modified) were tested. Throughout the text and figures, "Ref" and "P" denote the reference and modified laminates, respectively.

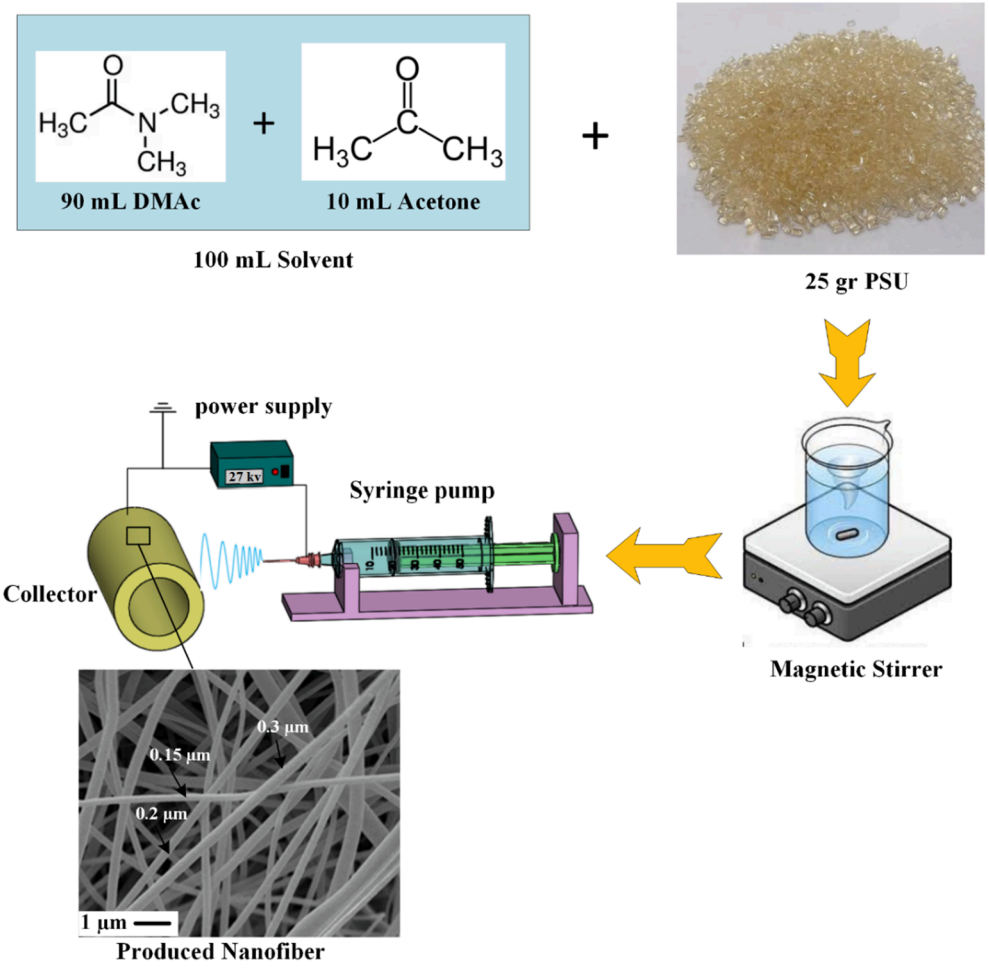

Fig. 1. Manufacturing PSU nanofiber through the electrospinning method.

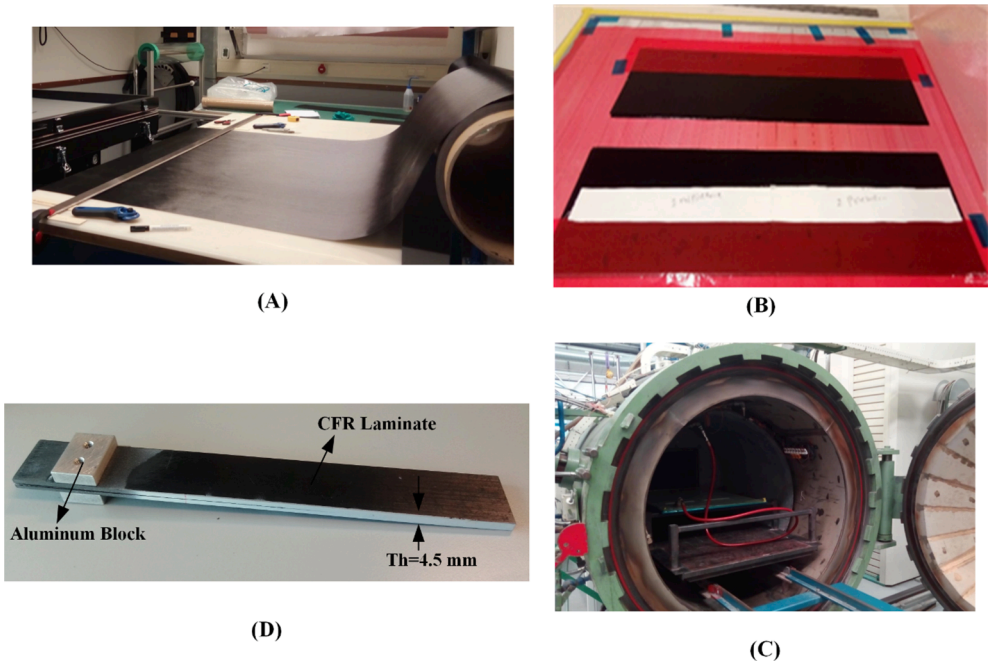

Fig. 2. The manufacturing of composite specimens: **A)** prepreg cutting **B)** laminating of prepreg and PSU nanofiber **C)** curing in autoclave, and **D)** The produced specimen.

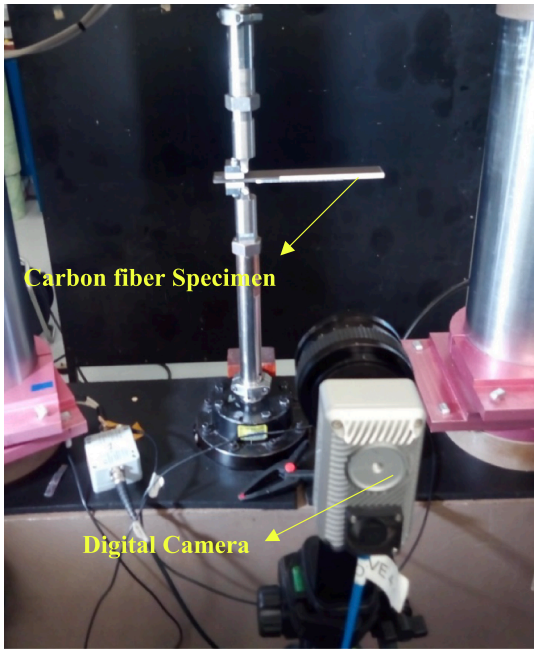

Fig. 3. Procedure of mode-I fracture test.

3.2. Fatigue test procedure

Fatigue test was performed following the ASTM D6115 standard [9] under displacement-control condition. The specimens underwent sinusoidal cyclic loading at a frequency of 5 Hz with a cyclic displacement ratio (R) of 0.3, where R is the ratio of the minimum displacement (δ_{min}) to the maximum displacement (δ_{max}). During the test, cycle count, displacement and load, were continuously measured and recorded to plot fatigue curves. The fatigue test was terminated after 100,000 cycles for each specimen. Visual crack length assessment was executed using a digital camera with a resolution of 4 MP and a frame rate of 55 fps, which was provided by OPTOMOTIVE Company. To capture images of the crack tip, the fatigue machine automatically stopped after every 1000 cycles, went to the adjusted maximum displacement, and triggered the camera. Once the photo was taken, the fatigue test was resumed to continue testing the specimens.

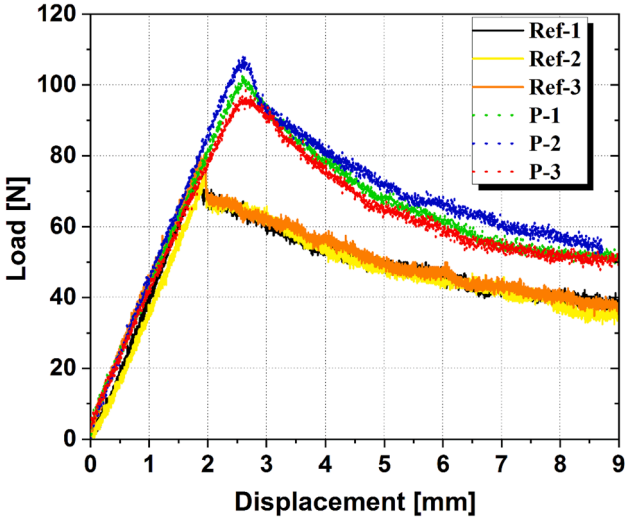

Fig. 4. The result of quasi-static tests for all specimens.

4. Quasi-static results

Fig. 4 illustrates the load–displacement graphs of all quasi-static test specimens. Importantly, it should be noted that the slopes of the curves remain consistent for all specimens prior to the initiation of cracks, indicating that the inclusion of nanofibers does not affect the slope. In other words, the effective modulus of all specimens is the same.

As seen in Fig. 4, once the load reached the maximum (P_{cr}), the crack initiated and subsequently the load started to decrease. The average maximum load values were determined to be 80 N for the reference specimens and 103 N for the modified specimens, indicating a significant improvement of 30%. It is worth mentioning that the reference specimens exhibited a sudden decrease in load, which can be attributed to the presence of a resin-rich region at the initial delamination point. This behavior may indicate a rapid expansion of the crack length. In contrast to the reference specimens, the sudden drop in load–displacement curve was prevented in the modified specimens due to the presence of PSU nanofibers. As a result, the load decreased gradually in these specimens, and the compliance increased at the critical moment when the crack began to propagate. An increase in compliance is a desirable property for structures as it helps to prevent sudden crack growth and catastrophic failure.

The ASTM-D5528 standard prescribes the use of equation (1) to calculate the fracture toughness (G_{IC}).

$$G_{IC} = \frac{3p_{cr}\delta_{cr}}{2B(a_0 + \Delta)} \tag{1}$$

In this equation, the parameter Δ is used to indicate the effective delamination extension for adjusting the rotation of beam arms at the crack front, where a_0 is the initial delamination length, p_{cr} represents the maximum force, δ_{cr} is the corresponding displacement, and B is the width of the specimen as shown in Fig. 2-d. To determine the value of Δ, several points need to be selected from the section of continuous crack growth in the force–displacement diagram. At these points, the corresponding displacement (δ), force (P), and crack length (a) values are recorded. The compliance (C) is determined by dividing the displacement by the force at each point. Subsequently, the third root of compliance ($C^{1/3}$) is calculated and plotted against the crack length. A linear relationship is obtained by fitting a line to these two parameters. Fig. 5 depicts the linear correlation between these two parameters, along with the values of Δ for both the reference (Ref-3) and modified (P-3) specimens.

All fracture test specimens' key parameters and fracture toughness values are presented in Table 1. The results demonstrate that the average fracture toughness for the reference specimens is 0.182 kJ/m2, whereas for the modified specimens, it is 0.334 kJ/m2. This shows a substantial 84% improvement in fracture toughness attributed to the incorporation of polysulfone nanofibers.

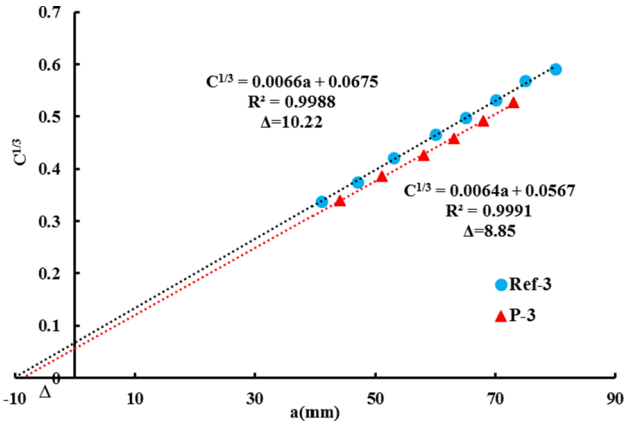

Fig. 5. Calculation of Δ Parameter for Reference and Modified Specimens.

Table 1
Fracture test parameters and calculated fracture toughness values for all specimens.

Samples	P_{cr} (N)	δ_{cr}	B (mm)	a_0 (mm)	Δ (mm)	G_{IC} (kJ/m^2)	P_{cr} (Ave.)	δ_{cr} (Ave.)	Δ (Ave.)	G_{IC} (Ave.)
Ref-1	84.77	1.87	25.07	40	8.38	0.196	80	1.92	10.60	0.182
Ref-2	74.58	1.94	25.1	40	13.31	0.162				±0.017
Ref-3	80.6	1.95	25.01	40	10.22	0.188				
P-1	102.5	2.62	25.05	40	8.94	0.330	103	2.61	8.22	0.334
P-2	108.2	2.60	25.09	40	6.89	0.363				±0.022
P-3	98.5	2.63	25.08	40	8.85	0.320				

5. Fatigue test results

As mentioned in section 3.2, the fatigue test was conducted in accordance with the ASTM D6115 standard [9] under displacement-control conditions. To determine the minimum and maximum displacement in each cyclic test as fatigue parameters, Equation (2) was employed. This equation involved selecting a G_{Iimax}/G_{IC} parameter of 0.81, where G_{Iimax} represents the maximum energy release rate at the first cycle. In addition, the δ_{cr} parameter for both the reference and modified specimens is known, with values of 1.92 mm and 2.61 mm, respectively, as presented in Table 1. So by applying Equation (2), the value of δ_{max} was calculated. Furthermore, by considering the known R value ($\delta_{min}/\delta_{max} = 0.3$), the minimum displacement (δ_{min}) as a fatigue input parameter was determined. Table 2 displays the fatigue test parameters for each specimen type.

$$\frac{G_{Iimax}}{G_{IC}} = \left(\frac{\delta_{\max}}{\delta_{cr}}\right)^2 \tag{2}$$

As shown in Fig. 6, because of the displacement-control condition, the values of δ_{min} and δ_{max} didn't change throughout the fatigue testing, while P_{min} and P_{max} gradually decreased as the number of cycles increased.

Fig. 7 presents the relationship between crack growth and the number of cycles for the P-5 specimen. It can be observed that the crack growth rate during the first 10,000 cycles is significantly higher than in the subsequent cycles.

In order to determine the amount of fatigue crack growth, the compliance method was utilized. The calculation of compliance and subsequent crack length were done using equations (3) and (4):

$$C_i = \left(\frac{\delta_{\max}}{P_{\max}}\right)_i \tag{3}$$

$$a_i = \frac{C_i^{\frac{1}{3}}}{0.0064} - \Delta_{ave} \tag{4}$$

The compliance method was employed to calculate the fatigue crack length (a_i) based on the relationship between compliance and the crack length. The average crack length-modified parameter (Δ_{ave}) obtained from the quasi-static tests (refer to Table 1) was also considered. To verify the accuracy of the compliance method, the crack length was also determined using the digital camera. Fig. 8 demonstrates the calculated crack length (a) using both methods, indicating a strong agreement between them.

The crack growth rate (da/dN) was calculated following the guidelines outlined in the ASTM E647 standard [37]. The secant method was utilized, which involves determining the slope of the straight line connecting two consecutive data points. It is defined more precisely as follows:

$$\left(\frac{da}{dN}\right)_i = \frac{a_{i+1} - a_i}{N_{i+1} - N_i} \tag{5}$$

In this equation the crack length and cycle count are denoted by a_i and N_i, respectively. The subsequent data point is represented as a_{i+1}, with its corresponding cycle count as N_{i+1}. The maximum energy release rate (G_{Imax}) for each cycle was determined using Eq. (6), as follows:

$$(G_{Imax})_i = \frac{3(p_{\max})_i \delta_{\max}}{2B(a_i + \Delta_{ave})} \tag{6}$$

Fig. 9 displays the variation of energy release rate (G_{Imax}) and fatigue crack growth rate (da/dN) as a function of cycles for the P-5 specimen. It is observed that both parameters exhibit a decreasing trend with increasing number of cycles. The figure indicates that there is a substantial reduction in the crack growth rate during the initial 10,000 cycles compared to the later cycles. This observation agrees with the results obtained using the digital camera recording.

In Fig. 10, the relationship between da/dN and G_{Imax} is plotted on a doble logarithmic scale.

It is evident that the modified samples require more energy for a constant crack growth rate compared to the reference samples. This indicates a significant improvement in the resistance to fatigue crack growth in the modified specimens. This behavior can be described by the Paris law, which establishes a power relationship between the maximum energy release rate and crack growth rate, as expressed below [38]:

$$\frac{da}{dN} = k(G_{Imax})^m \tag{5}$$

The coefficients k and m in the Paris equation are calculated by

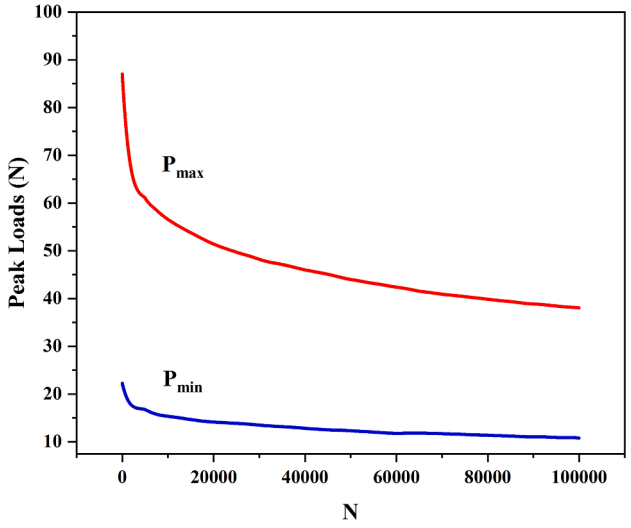

Fig. 6. Reduction of the maximum and minimum loads in P-5 test specimen during the fatigue cycles.

Table 2
Sample specifications and selected parameters for the fatigue test.

Samples	a_0 (mm)	B (mm)	G_{Iimax}/G_{IC}	$R = \delta_{min}/\delta_{max}$	δ_{min} (N)	δ_{max} (N)
Ref-4	40	25.07	0.8	0.3	0.51	1.71
Ref-5	40	25.08	0.8	0.3	0.51	1.71
P-4	40	25.08	0.8	0.3	0.7	2.33
P-5	40	25.05	0.8	0.3	0.7	2.33

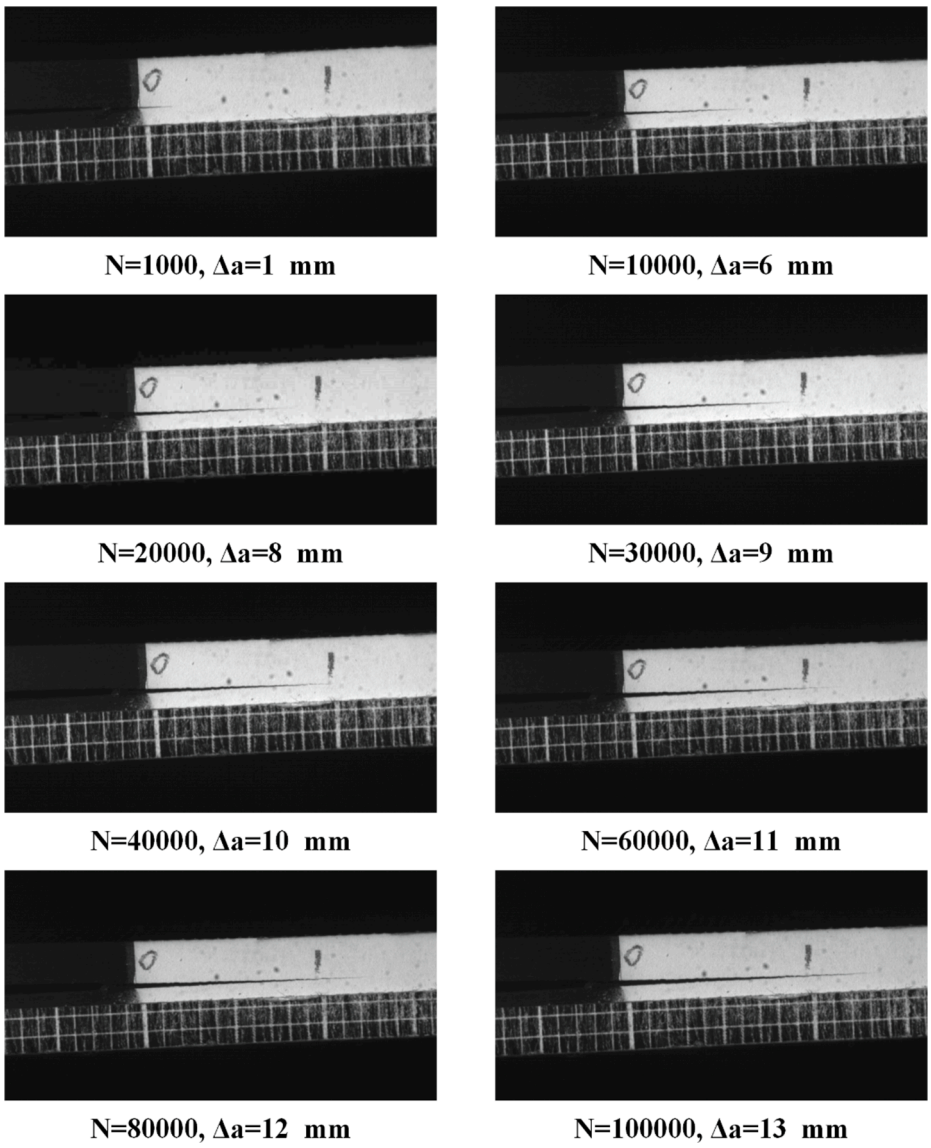

Fig. 7. Detection of the fatigue crack growth in P-5 test specimen using a digital camera.

fitting a line through the data points using the least squares method. As shown in Fig. 10 the m values for the PSU modified and reference samples were determined to be 3.39 and 9.71, respectively. This finding suggests that the presence of polysulfone caused a slope reduction of the da/dN-G_{Imax} graphs. It is apparent from the figure that the rate of fatigue crack growth in the reference samples is notably greater than in the modified ones. For example, when the G_{Imax} is equivalent to 130 J/m^2, the value of da/dN is 1.65e-7 m/cycle and 1.49e-6 m/cycle for the modified and reference specimens, respectively. This result provides evidence that the rate of fatigue crack growth is significantly slower in the modified samples, approximately 9 times slower. Table 3 provides a comparative analysis of calculated fatigue crack growth rates at different G_{Imax} values (ranging from 92 to 150 J/m^2). The results indicate that as the G_{Imax} values increase, the impact of nanofibers becomes increasingly pronounced. This is evident from the considerably higher coefficient of f, representing the ratio of crack growth rate in the reference specimens to that in the modified specimens. So the influence of nanofibers becomes more pronounced as the values of G_{Imax} increase.

6. The SEM results

Fig. 11 presents SEM pictures depicting the fractured surfaces of specimens under quasi-static conditions. As illustrated in Fig. 11-A, a region characterized by an abundance of resin can be observed at the initial crack propagation area in the reference specimen. In contrast, this resin-rich region is not present in the modified specimen (Fig. 11-C). Consequently, when analyzing the displacement force behavior, the modified specimens exhibited an elevated level of compliance. Conversely, in the reference specimens, the existence of the resin-rich area resulted in a sudden decline in strength.

Moreover in the reference samples, the fracture surface exhibits a brittle nature, with notable failure modes including fiber breakage, matrix cracking, and fiber/matrix debonding. The fracture surface shown in Fig. 11-B exhibits distinct fiber imprints resulting from the aforementioned debonding. Conversely, in the PSU-modified laminates shown in Fig. 11-C and 11-D, the interface layer experienced phase separation, leading to the creation of a distinct sea-island region composed of PSU and epoxy constituents. These findings suggest that within the continuous epoxy phase, spherical PSU particles are present, as visually indicated by the yellow arrows in the accompanying image. The high viscosity of PSU, a thermoplastic polymer, prevents the generated spheres from deviating significantly from the original nanofiber direction and maintains their initial positions [19]. Based on the analysis of SEM images, the improved fracture toughness associated

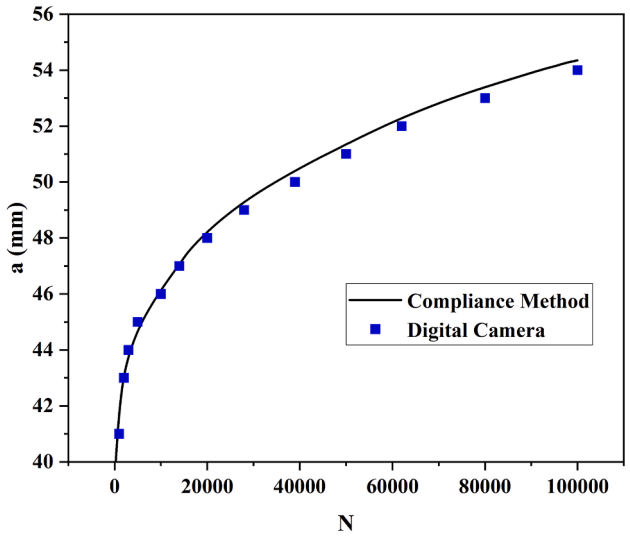

Fig. 8. Calculation of the crack length using two different methods (P-5 test specimen).

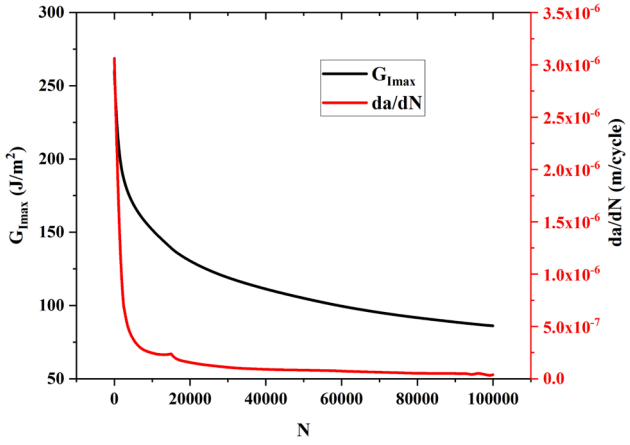

Fig. 9. The variation of fatigue crack growth rate and energy release rate during the cycles (P-5).

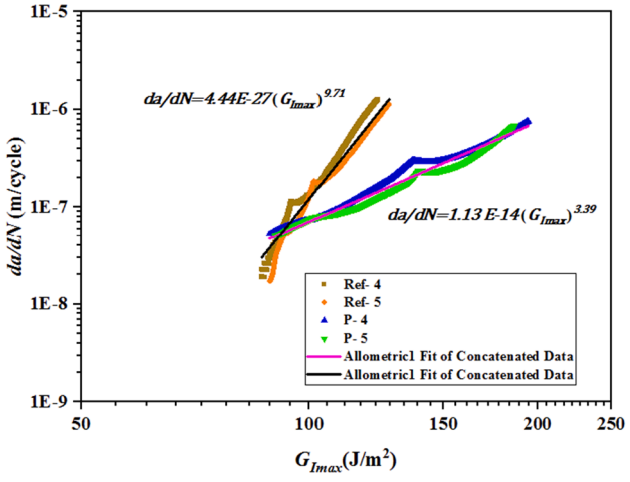

Fig. 10. Double-log plots of da/dN vs. G_{Imax} for the investigated specimens.

Table 3
Comparative analysis of the rate of fatigue crack growth at different G_{Imax} values.

G_{Imax} (J/m^2)	da/dN (m/cycle)		The ratio of crack growth rate (f)
	Reference	Modified	
92	5.19712E-08	5.13E-08	1.01
100	1.16784E-07	6.81E-08	1.72
110	2.9465E-07	9.41E-08	3.13
120	6.85856E-07	1.26E-07	5.43
130	1.49201E-06	1.66E-07	9.00
140	3.06398E-06	2.13E-07	14.38
150	5.98727E-06	2.69E-07	22.24

with PSU can be attributed to the following mechanisms:

1- The pull-out of PSU particles leads to the formation of numerous core and cavity shapes, represented by the red and yellow arrows, respectively. These particles create bridges between adjacent layers, effectively absorbing energy during their displacement from one layer to another.
2- The presence of PSU microspheres contributes to crack deflection during delamination. Due to the higher toughness of PSU compared to epoxy, the cracks are redirected instead of propagating through the PSU particles. This mechanism enhances energy absorption, resulting in an increased fracture toughness (G_{IC}). These two mechanisms are schematically illustrated in Fig. 12.
3- The localized plastic deformation observed in the PSU, represented by the light areas indicated by the blue arrows in Fig. 11-D, can be attributed to its thermoplastic nature. This deformation played a significant role in absorbing energy.

Fig. 13 illustrates fracture surfaces of the fatigue tests, comparing the reference and modified specimens. One of the failure mechanisms observed on the fracture surfaces is known as the "scarp" phenomenon [39]. This mechanism involves the formation of micro cracks within the matrix, located ahead of the crack front and occurring on various planes. Subsequently, these micro cracks converge onto a single plane. Typically, localized cracking develops in regions susceptible to initiation, such as around the fibers, and extends through the surrounding resins.

Due to the growth of cracks in different planes, they ultimately intersect and form distinct sharp edges referred to as scarps. These scarps exhibit alignment parallel to the fibers, generally following their direction. In Fig. 13-A, these scarps are visually represented as prominent white edges. Notably, matrix micro cracks initiate at the fiber intersections and propagate as "textured micro flow" inclined towards the primary direction of crack growth within the matrix and at the intersection points of the scarps. This characteristic sharpness is consequently generated. Moreover, the orientation of textured micro flow lines observed within matrix microcracks can be utilized as a method to anticipate the path of propagation for the main crack.

The mode I fatigue failure surfaces also exhibit another notable phenomenon known as striation [40]. These striation patterns emerge because of cyclic fatigue on the fracture surfaces, manifesting either on the matrix or the fibers. These patterns form parallel to each other and perpendicular to the direction of crack growth. Typically, striations appear as thin lines, varying in lightness or darkness.

The mechanism behind the formation of these lines involves the initial appearance of cracks between the fiber and the matrix. Subsequently, these cracks continue to propagate and extend. The expansion of these cracks does not occur entirely perpendicular to the fiber direction; instead, they tend to grow in alignment with the primary crack growth direction. Consequently, when observed under a microscope, the striation lines appear curved. Moreover, the spacing between these striation lines can provide valuable information about the rate of fatigue crack growth. Actually, with each cycle, a new line is formed, and the

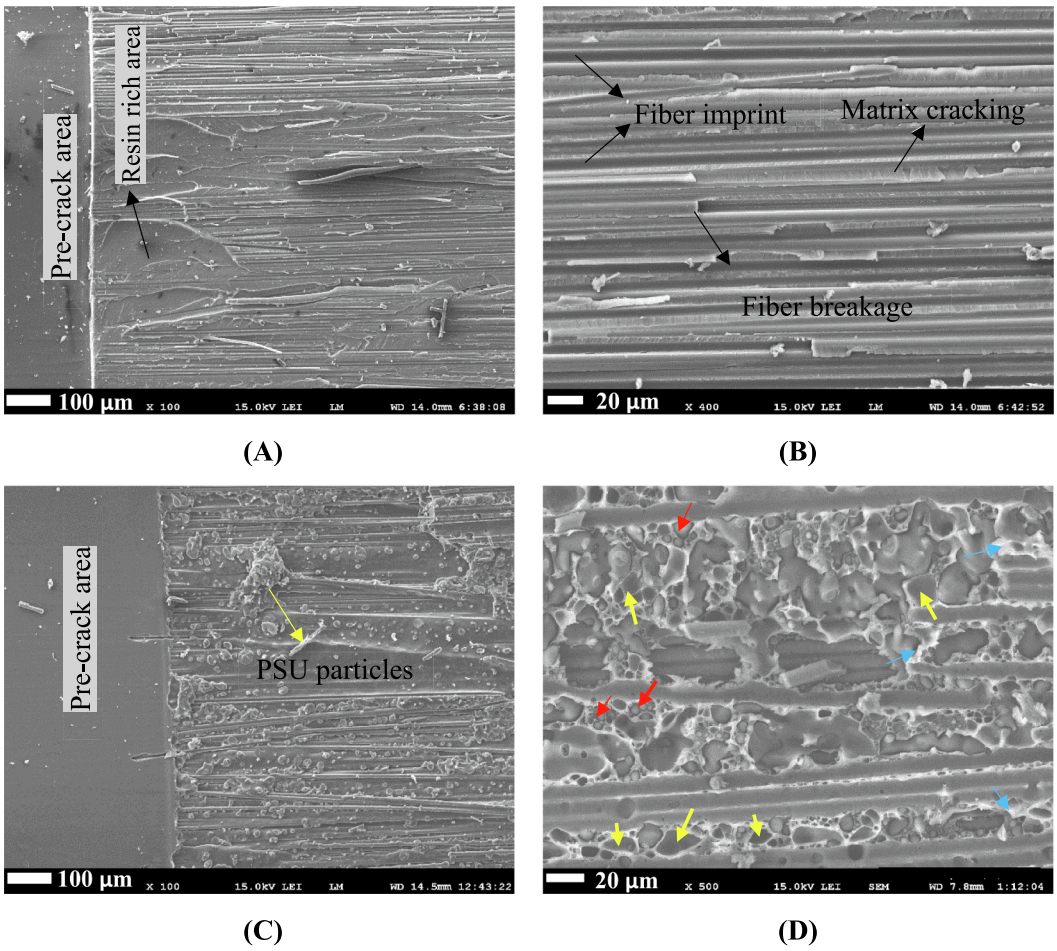

Fig. 11. The SEM micrograph of fracture surface of quasi-static specimes **A,B)** reference **C,D)** PSU-modified.

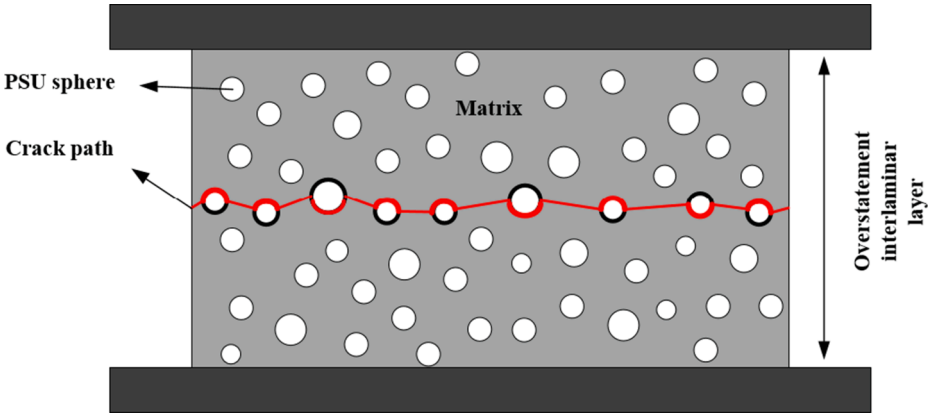

Fig. 12. The schematic of crack deflection mechanism by PSU particles.

distance between these lines serves as a valuable indicator of the rate at which the crack is growing.

Based on the observation in Fig. 13-B, which presents the fatigue micrograph of PSU modified specimens, none of the aforementioned failure mechanisms are apparent in these particular specimens. The presence of PSU nanofibers acts as an impediment, preventing the continuous and regular micro cracks growth, thus inhibiting the formation of scarp and striation lines. In other words, the steady and continuous growth of this micro cracks and then the formation of scarp and striation lines is considered a kind of resonance phenomenon, in which the presence of PSU nanofibers interrupts this chain.

Furthermore, upon comparing Fig. 13-A and B, it becomes evident that both figures exhibit visible carbon fiber imprints, thus indicating the occurrence of fiber/matrix debonding. In the reference specimens, the fiber imprints appear remarkably smooth and continuous, implying weak adhesion between the epoxy and fibers, facilitating easy separation of the fiber from the resin. Conversely, the modified specimens exhibit fiber imprints with an uneven and discontinuous surface. This study demonstrates that the presence of nanofibers effectively hinders the fiber/matrix debonding mechanism, resulting in improved adhesion between the fibers and the matrix. This enhancement can be attributed to the strong adhesive properties of the polymeric sizing of the carbon

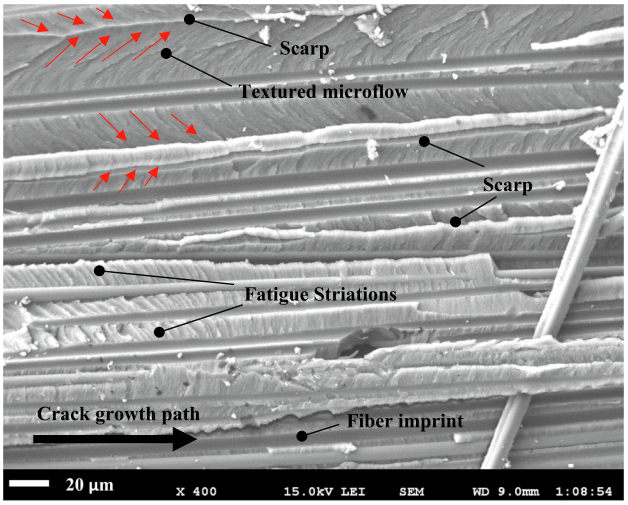

(A)

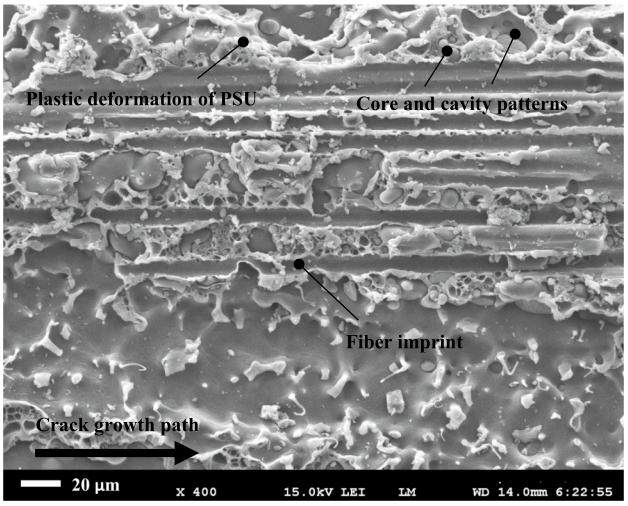

(B)

Fig. 13. SEM micrograph of fracture surface of fatigue sampless **A)** reference **B)** PSU-modified.

fiber with PSU. Consequently, this finding should be considered for future research endeavors.

7. Conclusion

In this investigation, the mode-I fatigue performance of carbon/epoxy laminates was studied with the incorporation of a 100-µm electrospun nanofibrous mat (PSU) between mid-layers. The fatigue tests maintained consistent energy release ratios and G_{Iimax}/G_{IC} values ($\delta_{min}/\delta_{max}$ = 0.3 and 0.8, respectively). The findings reveal an 85% enhancement in fracture toughness, because of introducing PSU nanofibers. The fatigue plots demonstrated that the inclusion of PSU nanofiber resulted in a notable reduction in the slope of the G_{Imax} - da/dN curve. This reduction in slope indicated a significant decrease in the fatigue crack growth rate (da/dN) for the modified specimens. In fact, the fatigue crack growth rate was reduced by up to 22 times compared to the unmodified specimens. The utilization of scanning electron microscopy (SEM) allowed for the characterization of damage and toughening mechanisms, uncovering that nanofibers contribute to the improvement in mechanical properties through bridging between layers at the crack tip, crack deflection, plastic deformation due to their thermoplastic nature. Moreover, the SEM micrograph analysis revealed that the inclusion of PSU nanofibers functions as a successful deterrent against primary fatigue failure mechanisms, including scarp lines, striation patterns, and fiber–matrix debonding. This beneficial effect leads to a notable decrease in the fatigue crack growth rate.

CRediT authorship contribution statement

Reza Mohammadi: Conceptualization, Methodology, Writing – original draft, Supervision. **Roya Akrami:** Writing – review & editing, Supervision. **Maher Assaad:** Writing – review & editing. **Mohamed Nasor:** Writing – review & editing. **Ahmed Imran:** Conceptualization, Writing – review & editing, Funding acquisition. **Mohammad Fotouhi:** Conceptualization, Methodology, Writing – review & editing, Funding acquisition.

Declaration of Competing Interest

The authors declare that they have no known competing financial interests or personal relationships that could have appeared to influence the work reported in this paper.

Data availability

The authors do not have permission to share data.

Acknowledgements

This work was partially funded by Ajman University (2022-IRG-ENIT-12) and the UK Engineering and Physical Sciences Research Council (EP/V009451/1). The data necessary to support the conclusions are included in the paper.

References

[1] Z. Li, Z. Wang, Effect of interlayer carbon nanotube films on the quasi-static and dynamic mode I fracture behavior of laminated composites – an experimental and numerical investigation, Theor. Appl. Fract. Mech. 125 (2023) 103932.
[2] T. Laux, R.C. Bullock, O.T. Thomsen, J.M. Dulieu-Barton, Lay-up effect on the open-hole shear strength of composite laminates, Compos. Sci. Technol. 239 (2023) 110044.
[3] L. Yao, J. Liu, Z. Lyu, R.C. Alderliesten, C. Hao, C. Ren, L. Guo, In-situ damage mechanism investigation and a prediction model for delamination with fibre bridging in composites, Eng. Fract. Mech. 281 (2023) 109079.
[4] P. Shabani, L. Li, J. Laliberte, G. Qi, D. Rapking, D. Mollenhauer, High-fidelity simulation of low-velocity impact damage in fiber-reinforced composite laminates using integrated discrete and continuum damage models, Compos. Struct. 313 (2023) 116910.
[5] M. Saeedifar, H. Hosseini Toudeshky, The Effect of Interlaminar and Intralaminar Damage Mechanisms on the Quasi-Static Indentation Strength of Composite Laminates, Appl. Compos. Mater. 30 (3) (2023) 871–886.
[6] M. Saeedifar, H. Saghafi, R. Mohammadi, D. Zarouchas, Temperature dependency of the toughening capability of electrospun PA66 nanofibers for carbon/epoxy laminates, Compos. Sci. Technol. 216 (2021) 109061.
[7] R. Mohammadi, M.A. Najafabadi, H. Saghafi, D. Zarouchas, Mode-II fatigue response of AS4/8552 carbon /epoxy composite laminates interleaved by electrospun nanofibers, Thin-Walled Struct. 154 (2020) 106811.
[8] X. Cheng, J. Ying, Z. Wu, L. Shi, X. Hu, Mode I interlaminar fracture characteristics of CNTs doped woven and unidirectional CFRP via acoustic emission, Theor. Appl. Fract. Mech. 124 (2023) 103812.
[9] R. Palazzetti, A. Zucchelli, Electrospun nanofibers as reinforcement for composite laminates materials – A review, Compos. Struct. 182 (2017) 711–727.
[10] R. Mohammadi, M. Ahmadi Najafabadi, H. Saghafi, M. Saeedifar, D. Zarouchas, A quantitative assessment of the damage mechanisms of CFRP laminates interleaved by PA66 electrospun nanofibers using acoustic emission, Compos. Struct. 258 (2021) 113395.
[11] M. Povolo, E. Maccaferri, D. Cocchi, T.M. Brugo, L. Mazzocchetti, L. Giorgini, A. Zucchelli, Damping and mechanical behaviour of composite laminates interleaved with rubbery nanofibers, Compos. Struct. 272 (2021) 114228.
[12] R.E. Neisiany, S.N. Khorasani, J.K.Y. Lee, M. Naeimirad, S. Ramakrishna, Interfacial toughening of carbon/epoxy composite by incorporating styrene acrylonitrile nanofibers, Theor. Appl. Fract. Mech. 95 (2018) 242–247.
[13] T. Brugo, G. Minak, A. Zucchelli, X.T. Yan, J. Belcari, H. Saghafi, R. Palazzetti, Study on Mode I fatigue behaviour of Nylon 6,6 nanoreinforced CFRP laminates, Compos. Struct. 164 (2017) 51–57.
[14] H. Saghafi, A.R. Moallemzadeh, A. Zucchelli, T.M. Brugo, G. Minak, Shear mode of fracture in composite laminates toughened by polyvinylidene fluoride nanofibers, Compos. Struct. 227 (2019) 111327.

[15] E. Maccaferri, M. Dalle Donne, L. Mazzocchetti, T. Benelli, T.M. Brugo, A. Zucchelli, et al., Rubber-enhanced polyamide nanofibers for a significant improvement of CFRP interlaminar fracture toughness, Sci. Rep. 12 (2022) 21426.
[16] P.K. Barzoki, M. Latifi, A.M. Rezadoust, The outstanding effect of nanomat geometry on the interlaminar fracture toughness behavior out of autoclave made glass/phenolic composites under mode-I loading, Eng. Fract. Mech. 205 (2019) 108–119.
[17] P.K. Barzoki, A.M. Rezadoust, M. Latifi, H. Saghafi, G. Minak, Effect of nanofiber diameter and arrangement on fracture toughness of out of autoclave glass/phenolic composites - Experimental and numerical study, Thin-Walled Struct. 143 (2019) 106251.
[18] N. Zheng, Y. Huang, H.-Y. Liu, J. Gao, Y.-W. Mai, Improvement of interlaminar fracture toughness in carbon fiber/epoxy composites with carbon nanotubes/polysulfone interleaves, Compos. Sci. Technol. 140 (2017) 8–15.
[19] S. Cai, Y. Li, H.-Y. Liu, Y.-W. Mai, Effect of electrospun polysulfone/cellulose nanocrystals interleaves on the interlaminar fracture toughness of carbon fiber/epoxy composites, Compos. Sci. Technol. 181 (2019) 107673.
[20] A. Gholizadeh, H. Mansouri, A. Nikbakht, H. Saghafi, M. Fotouhi, Applying Acoustic Emission Technique for Detecting Various Damages Occurred in PCL Nanomodified Composite Laminates, Polymers 13 (21) (2021) 3680.
[21] M. Khandaker, H. Nomhwange, H. Progri, S. Nikfarjam, M.B. Vaughan, Evaluation of Polycaprolactone Electrospun Nanofiber-Composites for Artificial Skin Based on Dermal Fibroblast Culture, Bioengineering 9 (1) (2022) 19.
[22] X. Song, J. Gao, N. Zheng, H. Zhou, Y.-W. Mai, Interlaminar toughening in carbon fiber/epoxy composites interleaved with CNT-decorated polycaprolactone nanofibers, Compos. Commun. 24 (2021) 100622.
[23] S. Hamer, H. Leibovich, A. Green, R. Avrahami, E. Zussman, A. Siegmann, D. Sherman, Mode I and Mode II fracture energy of MWCNT reinforced nanofibrilmats interleaved carbon/epoxy laminates, Compos. Sci. Technol. 90 (2014) 48–56.
[24] L. Daelemans, A. Cohades, T. Meireman, J. Beckx, S. Spronk, M. Kersemans, I. De Baere, H. Rahier, V. Michaud, W. Van Paepegem, K. De Clerck, Electrospun nanofibrous interleaves for improved low velocity impact resistance of glass fibre reinforced composite laminates, Mater. Des. 141 (2018) 170–184.
[25] A. Gholizadeh, M.A. Najafabadi, H. Saghafi, R. Mohammadi, Considering damages to open-holed composite laminates modified by nanofibers under the three-point bending test, Polym. Test. 70 (2018) 363–377.
[26] T. Brugo, R. Palazzetti, The effect of thickness of Nylon 6,6 nanofibrous mat on Modes I-II fracture mechanics of UD and woven composite laminates, Compos. Struct. 154 (2016) 172–178.
[27] H. Salimi-Mofrad, A. Rahbar Ranji, H. Saghafi, Effect of electrospun PA66 nanofibrous mat thickness on mode-II fracture toughness using acoustic emission (AE) with data clustering technique, Theor. Appl. Fract. Mech. 124 (2023) 103788.
[28] R. Mohammadi, M.A. Najafabadi, H. Saghafi, D. Zarouchas, Fracture and fatigue behavior of carbon/epoxy laminates modified by nanofibers, Compos. A Appl. Sci. Manuf. 137 (2020) 106015.
[29] A. Gholizadeh, M.A. Najafabadi, H. Saghafi, R. Mohammadi, Considering damage during fracture tests on nanomodified laminates using the acoustic emission method, Eur. J. Mech. A. Solids 72 (2018) 452–463.
[30] L. Daelemans, S. van der Heijden, I. De Baere, H. Rahier, W. Van Paepegem, K. De Clerck, Nanofibre bridging as a toughening mechanism in carbon/epoxy composite laminates interleaved with electrospun polyamide nanofibrous veils, Compos. Sci. Technol. 117 (2015) 244–256.
[31] R. Palazzetti, Flexural behavior of carbon and glass fiber composite laminates reinforced with Nylon 6,6 electrospun nanofibers, J. Compos. Mater. 49 (27) (2015) 3407–3413.
[32] K. Magniez, C. De Lavigne, B.L. Fox, The effects of molecular weight and polymorphism on the fracture and thermo-mechanical properties of a carbon-fibre composite modified by electrospun poly (vinylidene fluoride) membranes, Polymer 51 (12) (2010) 2585–2596.
[33] H. Saghafi, A. Nikbakht, R. Mohammadi, D. Zarouchas, The Thickness Effect of PSF Nanofibrous Mat on Fracture Toughness of Carbon/Epoxy Laminates, Materials. 14 (2021) 3469.
[34] H. Saghafi, R. Palazzetti, H. Heidary, T.M. Brugo, A. Zucchelli, G. Minak, Toughening Behavior of Carbon/Epoxy Laminates Interleaved by PSF/PVDF Composite Nanofibers, Appl. Sci. 10 (2020) 5618.
[35] HexPly ® 8552 Epoxy matrix (180°C/356°F curing matrix) in FTA 072e, Hexcel Composites Publication 2013.
[36] Q.i. Chen, Y. Zhao, Z. Zhou, A. Rahman, X.-F. Wu, W. Wu, T. Xu, H. Fong, Fabrication and Mechanical Properties of Hybrid Multi-Scale Epoxy Composites Reinforced with Conventional Carbon Fiber Fabrics Surface-Attached with Electrospun Carbon Nanofiber Mats, Compos. B Eng. 44 (1) (2013) 1–7.
[37] T.K. O'brien, Delamination of Composite Materials, Compos Mater. 4 (1991) 181.
[38] Y. Gong, L. Zhao, J. Zhang, N. Hu, A novel model for determining the fatigue delamination resistance in composite laminates from a viewpoint of energy, Compos. Sci. Technol. 167 (2018) 489–496.
[39] E. Greenhalgh, Failure Analysis and Fractography of Polymer Composites, Woodhead Publishing Series in Composites Science and Engineering. (2009) 1–595.
[40] V. Kaushik, A. Ghosh, Experimental and numerical investigation of Mode-I & Mode-II fatigue crack growth in unidirectional composites using XIGA-CZM approach, Int. J. Fatigue 134 (2020), 105461.